Linear and nonlinear dielectric spectroscopy in dipolar glasses

Alois Loidl, Joachim Hemberger, M. Winterlich, H. Ries, R. Böhmer

Angaben zur Veröffentlichung / Publication details:

Loidl, Alois, Joachim Hemberger, M. Winterlich, H. Ries, and R. Böhmer. 1996. "Linear and nonlinear dielectric spectroscopy in dipolar glasses." *Ferroelectrics* 176 (1): 43–59. https://doi.org/10.1080/00150199608223599.

LINEAR AND NONLINEAR DIELECTRIC SPECTROSCOPY IN DIPOLAR GLASSES

A. LOIDL,† J. HEMBERGER, M. WINTERLICH, H. RIES and R. BÖHMER‡

Institut für Festkörperphysik, Technische Hoschschule Darmstadt, 64289 Darmstadt, Germany

(Received June 26, 1995)

Two dipolar glass systems are investigated by broadband dielectric spectroscopy. The two systems under investigation, NH_4I:KI and solid solutions of deuterated betaine phosphate and betaine phosphite (BP:BPI), reveal very different freezing scenarios. The dielectric loss in NH_4I:KI is characterized by a power-law behavior on frequency $\varepsilon'' \sim \nu^r$, indicative for the near-equilibrium dynamics in the glass phase. The deuterated proton glass D-BP:BPI (40:60) exhibits a relaxational-type of freezing transition. Measurements of the nonlinear susceptibility and of the field cooled and zero-field cooled susceptibility provide clear evidence for a "static" dipolar glass transition at $T_g \sim 28$ K $\pm$ 2 K.

1. INTRODUCTION

Dipolar glasses (DG) are solids consisting of a regular lattice whose sites are randomly occupied by constituents containing dipole moments. These dipoles have orientational degrees of freedom, they interact with one another and, below some freezing temperature T_f, they freeze into random configurations. Molecular crystals without such randomness in their chemical constitution usually undergo an order-disorder phase transition from the paraelectric phase at high temperatures, where the dipole moments can reorient freely, into a phase with long-range electric order at low temperatures. The ferroelectric (FE) or antiferroelectric (AFE) order gets severely disturbed by dilution of the material with atomic species with no dipolar moments (type A phase diagram: Figure 1), or when one considers mixed crystals with FE and AFE order (type B phase diagram: Figure 2). In both cases, weak dilution very often stabilizes other types of long-range ordered structures, while strong enough dilution leads to a new type of phase, where the dipoles are cooperatively frozen-in devoid of long-range orientational order.

The qualitative description of dipolar glasses, which are a sub-species of orientational glasses (OG), is similar to spin glasses (SG). In SG random dilution of a magnetic species yields a new type of magnetic order (SG order) with many fascinating and unusual properties.[1] Meanwhile also extensive reviews on the experimental facts[2] and on the theory of OG[3] exist. The dipolar glass transition is interaction dominated and characterized by a cooperative freezing-in of the dipoles. Like in spin glasses, the interplay of frustrated interactions and site disorder plays a dominant role. The relevant parameters that determine the ground state properties are the

†Author to whom correspondence should be addressed.

‡Permanent address: Institut für Physikalische Chemie, Johannes Gutenberg-Universität, D-55099 Mainz, Germany.

strength of the average dipolar interaction, J, compared to the distribution width of the random interactions, Var(J). A dipolar glass phase exists for J/Var(J) < 1 and an ordered phase for J/Var(J) > 1. However, in addition to bond disorder mixed molecular compounds often reveal static random fields. Those are due to defect states which lead to spatially fluctuating electrostatic fields. Like bond disorder, also random fields have the tendency to suppress long-range orientational order.

Molecular alloys reveal two characteristic types of (x, T)-phase diagrams shown in Figures 1 and 2. In type A mixtures (Figure 1) the molecules carrying the dipole moment are substituted by non-polar atoms, molecules or ions. $(KOH)_x(KCl)_{1-x}$[4] and $(NH_4I)_x(KI)_{1-x}$[5] are prominent examples. Systems like $KTaO_3$ doped with Li, Nb etc.[6] also belong to this group. Here the dopant can perform hops between symmetry equivalent off-center positions, thereby polarizing the surrounding ions and establishing a reorienting dipole moment. For all x, these systems reveal dynamic orientational disorder at high temperatures. For large doping levels x, they exhibit order-disorder phase transitions at characteristic temperatures T_c. With decreasing

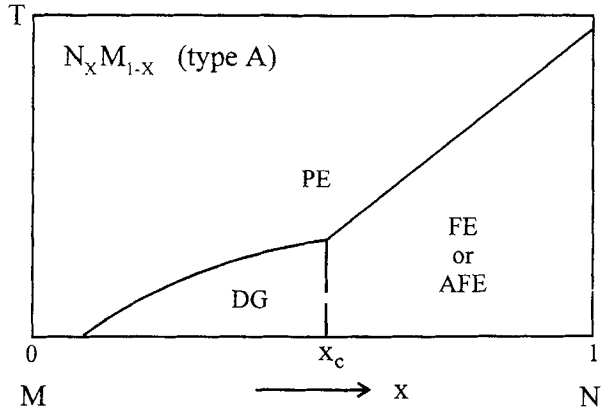

FIGURE 1 Schematic (x, T)-phase diagram of a N_xM_{1-x} crystal. N denotes a molecular compound characterized by orientational degrees of freedom, e.g. NH_4I, while M denotes a compound with no orientational degree of freedom, e.g. KI.

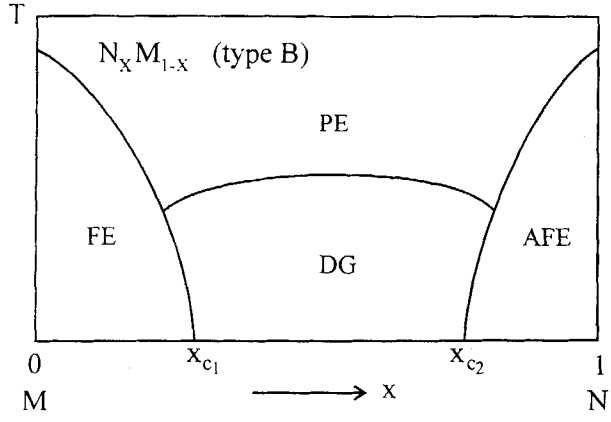

FIGURE 2 Schematic (x, T)-phase diagram of a N_xM_{1-x} mixed crystal. Both pure compounds reveal long-range electrical order. The high-temperature phase is paraelectric.

concentration of the component carrying the reorienting moment, the phase transition temperature decreases, and finally, below a critical concentration x_c long-range orientational order is fully suppressed. In this concentration range the molecular alloys undergo an orientational glass transition into a state of frozen-in orientational disorder. Phenomenologically the glass transition is a dynamical phenomenon and the freezing temperature sensitively depends on the time window of the experiment.

Another type of phase diagram (type B, Figure 2) is observed for molecular alloys made from components with competing interactions, as e.g. provided by mixtures of ferroelectric and antiferroelectric compounds: Solid solutions of KH_2PO_4 (KDP) type crystals like those from rubidium dihydrogen phosphate (RDP) and ammonium dihydrogen phosphate (ADP) are the most relevant examples. In these compounds, on dilution of either one of the pure compounds by the other the electric order is suppressed rapidly and a broad glassy regime evolves at intermediate concentrations.

In what follows, we discuss the dipolar freezing in a representative compound for each type of phase diagram. Dielectric spectroscopy on solid solutions of NH_4I:KI is discussed in detail. These compounds exhibit the type A phase diagram of dipolar systems. Mixtures of deuterated compounds of betaine phosphate (D-BP) and deuterated betaine phosphite (D-BPI) are prototypically discussed for the type B systems. We will show that the freezing scenarios are very different in these two classes of compounds. The complex dielectric permittivity of the former compound follows, as a function of frequency, a pure power-law behavior while in the latter compound it reveals predominantly relaxational behavior. This radically different behavior may result from different strengths of random bonds and random fields in the two compounds under consideration. In addition, we raise the question how to prove experimentally whether the system is characterized by a finite glass transition temperature. To answer this question we present results of the temperature dependence of the nonlinear susceptibility and of zero-field cooled (ZFC) and field-cooled (FC) measurements.

2. EXPERIMENTAL RESULTS

2.1 $(NH_4I)_x(KI)_{1-x}$

As a function of temperature and pressure the ammonium halides, NH_4Cl, NH_4Br and NH_4I undergo a sequence of order-disorder phase transitions.[8,9] In the generalized (p, T)-phase diagrams, so far α, β, γ and δ phases were known.[9] The high temperature α and β phases are dynamically disordered. The α modification is a NaCl-type structure in which the NH_4 ion is octahedrally coordinated by the surrounding iodide ions. It is generally believed that three hydrogens of the molecule are directed toward the I ions, while the fourth points towards one of the face centers of the octahedron. The cubic symmetry of this phase is stabilized via a fast reorientational motion of the NH_4 tetrahedron among eight symmetry-equivalent positions. The β modification is a CsCl-type structure in which the NH_4 molecules reorient between the two energetically equivalent orientations within the cube constituted by the surrounding I ions. The γ and δ phases reveal orientational order. In the γ phase octupolar order is established in a slightly distorted body centered cubic structure of tetragonal symmetry, while the δ modification shows an antiferrodistortive order of the molecules

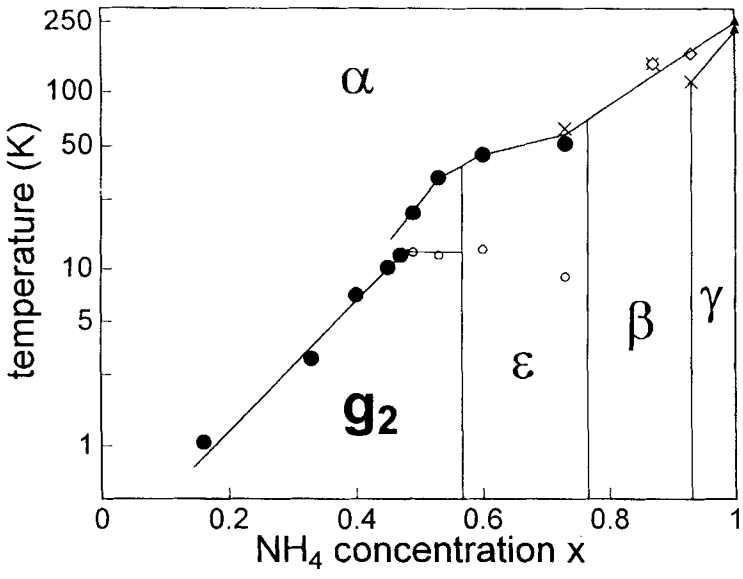

FIGURE 3 The (x, T)-phase diagram of $(NH_4)_x(KI)_{1-x}$. The high-temperature α phase is paraelectric. At low temperatures and with decreasing NH_4I concentration x the sequence γ, β and ε phase shows up. Below the critical concentration $x_c \sim 0.55$ two glass phases g_1 and g_2 develop (from Reference 6).

in a CsCl-type structure. The γ phase is the stable low-temperature structure of NH_4I. The δ phase can only be induced by high pressure.[8] It has been known since the early twenties that NH_4I and KI are completely miscible[10] and that a sufficient amount of potassium iodide stabilizes the high-temperature *fcc* structure.[11] Later on it has been suggested by neutron-scattering studies[12] and confirmed by dielectric spectroscopy[13] that $(NH_4I)_x(KI)_{1-x}$ forms an orientational glass below a critical concentration x_c. We have recently detected a new phase in $(NH_4I)_x(KI)_{1-x}$, which we called the ε phase.[14] The Bragg peaks indicative for the ε phase directly correspond to the diffuse scattered intensities which have been detected in deuterated glassy compounds by Berret *et al.*[15] and later on in $(NH_4I)_{0.5}(KI)_{0.5}$ by Umeki *et al.*[16] These diffusely scattered intensities, which indicate short range order only, appear close to the phase boundary of the ε phase. At the moment it is still unclear how far into the potassium-rich phase these short range order correlations can be observed. Finally we would like to mention that the relative strengths of random bonds and static random fields have been discussed on the basis of NMR experiments on deuterated[17] and protonated[18] samples with $x = 0.5$. Clearly more work is needed in this area before a microscopic understanding of the temperature and concentration dependence of the freezing process in the mixed ammonium halides can be achieved.

The phase diagram of $(NH_4I)_x(KI)_{1-x}$ which clearly is a representative of type A is shown in Figure 3 (Reference 6). This phase diagram reveals a rich variety of different low-temperature phases: with decreasing x, the sequence γ, β and ε phases can be observed. As stated above, the γ phase reveals complete orientational order in a slightly distorted CsCl structure. In the β phase, the NH_4 molecules still can reorient between two symmetry equivalent positions. The ε phase[14] reveals a complex polar order with a residual moment along the trigonal axis. Below the critical con-

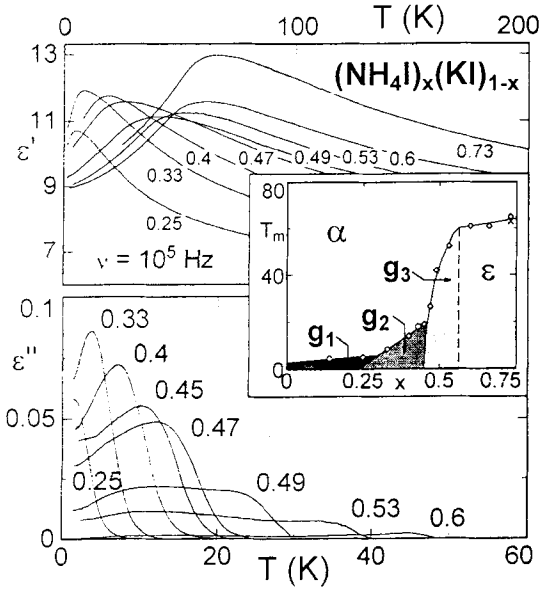

FIGURE 4 Temperature dependence of the dielectric constant ε_1 (upper frame) and of the dielectric loss ε_2 (lower frame) as measured at 100 kHz in $(NH_4I)_x(KI)_{1-x}$ for concentrations $x = 0.25$, 0.33, 0.4, 0.45, 0.47, 0.49, 0.53, 0.6 and 0.73. The inset shows the concentration dependence of the temperature of the peak maximum (T_m) of the real part of the dielectric constant. In addition to the paraelectric α phase and the orientationally ordered ε phase, three different glassy regimes, g_1, g_2 and g_3 show up.

centration $x_c \sim 0.55$ a glassy regime develops. It has been concluded from neutron scattering experiments, NMR studies and dielectric investigations that different glassy phases appear in $(NH_4I)_x(KI)_{1-x}$.[5] This phenomenon will be discussed later.

Here we present detailed and systematic investigations which show that the complex dielectric permittivity in this system can well be described by a power law behavior. Our results provide experimental evidence for the near-equilibrium dynamics of a molecular system in its glassy phase and can be used to test theoretical predictions dealing with a transition into a nonergodic ground state.

Figure 4 shows the temperature dependence of the dielectric constant ε_1 (upper frame) and of the dielectric loss ε_2 (lower frame) at a measuring frequency of 100 kHz, for different concentrations in $(NH_4I)_x(KI)_{1-x}$. With decreasing temperatures and for all concentrations investigated, ε_1 (T) reveals a Curie-Weiss-like increase, passes through a cusp-shaped maximum and finally decreases towards low temperatures. The temperature of the cusp maximum $T_m(x)$ exhibits a pronounced concentration dependence, a behavior that directly evidences that the freezing is interaction dominated. The loss phenomena (Figure 4, lower frame) are small and the temperature of the loss maxima, as well as the shape of the loss curves strongly depend on concentration; e.g., a single loss peak appears for concentrations $x \leq 0.45$, while double peak structures develop for higher x. For $x \geq 0.55$ the loss phenomena become very small.

For a closer inspection $T_m(x)$ is plotted in the inset of Figure 4. $T_m(x)$ depends weakly on x for NH_4I concentrations $x \geq 0.55$, but rapidly decreases in between $0.45 < x < 0.55$, followed by a linear decrease and finally by a smooth tailing-off

towards the lowest concentrations. For concentrations $0.55 < x < 0.8$ $(NH_4I)_x$ $(KI)_{1-x}$ exhibits the trigonal ε-phase in which the ammonium ions occupy two independent lattice sites in a complex orientationally ordered structure.[14] For $0.45 < x < 0.55$ the structure remains cubic with short range structural and orientational order, reminiscent of the ε-phase. It appears that the dielectric loss in the concentration regime $0.45 < x < 0.55$ indicates two subsequent anomalies. Finally, below concentrations $x = 0.45$ the NH_4 ions freeze-in randomly in a cubic *fcc* lattice.

The (x, T)-phase diagram (inset of Figure 4) reveals three distinct disordered low-temperature regimes, g_1, g_2 and g_3. For concentrations $0.45 < x < 0.55$ (g_3, light-shaded area), local ε-like distortions dominate. As discussed above, the loss in g_3 is small and exhibits a double peak structure. For $0.25 \leq x \leq 0.45$ (g_2, shaded area), well defined loss peaks develop. The transition line from the paraelectric high-temperature α phase to the glass state g_2 decreases linearly towards $x = 0.2$ which is the percolation limit of the *fcc* lattice. This behavior implies that the transition into the disordered state g_2 is dominated by next-nearest neighbor interactions. Finally, for $x < 0.25$, $T_m(x)$ depends only weakly on temperature. Hence, we conclude that the glassy regime g_1 (dark-shaded area) is dominated by relaxations of single NH_4 ions, only weakly disturbed by dipolar interactions. The disordered state g_1 is the regime in which the ammonium ions slow down in the Born-Mayer potential set up by the neighboring ions. The phase diagram of $(NH_4I)_x(KI)_{1-x}$ reveals a striking polymorphism of the crystalline phases, but, in addition, different amorphous states, which is even more striking. This means that the glassy state exists in different pockets in configurational space. This phenomenon has been called polyamorphism by Wolf *et al.*[19] and has been discussed in detail by Angell *et al.*[20] for glass forming liquids.

In what follows we will take a closer look at the glassy regime g_2 which exhibits, when compared to other dipolar glasses, very unusual dielectric features. The power-law behavior of the dielectric permittivity reveals that true equilibrium behavior can only be reached asymptotically slow.

Figure 5 shows the dispersive region of $\varepsilon_1(T)$ (upper frame) and $\varepsilon_2(T)$ (lower frame) in $(NH_4I)_{0.33}(KI)_{0.67}$ at three different measuring frequencies. The data are very similar to the complex magnetic susceptibility in the insulating spin glass $Eu_{0.4}Sr_{0.6}S$.[21] Especially the loss peaks do not show the characteristic features of a relaxational process (compare, e.g. with Figure 10). It seems that the mean relaxation rate is almost temperature independent.

In Figure 6 the frequency dependence of the dielectric loss is shown as $\log_{10}(\varepsilon'')$ vs $\log_{10}(\nu)$ for $x = 0.25$. Despite the fact that, due to the low losses of the material, the data points reveal large uncertainties at radio frequencies, a power-law behavior, namely $\varepsilon_2 \sim \nu^s$ is obeyed over six decades in frequency. Any description of these data in terms of a distribution of relaxation times needs a distribution function $g(\tau)$ covering at least 20 decades. The inset shows the frequency dependent data for $x = 0.33$ at audio frequencies. It is important to note that the data show no significant curvature in the log-log representations of Figure 6.

A power-law behavior in the frequency dependence of the dynamical susceptibility in the glass phase has been predicted by Sompolinsky and Zippelius[22] and by Fisher and Huse.[23] Sompolinsky and Zippelius (SZ)[22] have investigated dynamic properties of the Sherrington-Kirkpatrick model above and below the Almeida-Thouless (AT) line introducing a soft-spin version for Ising spins. Later on, Fischer and Kinzel[24]

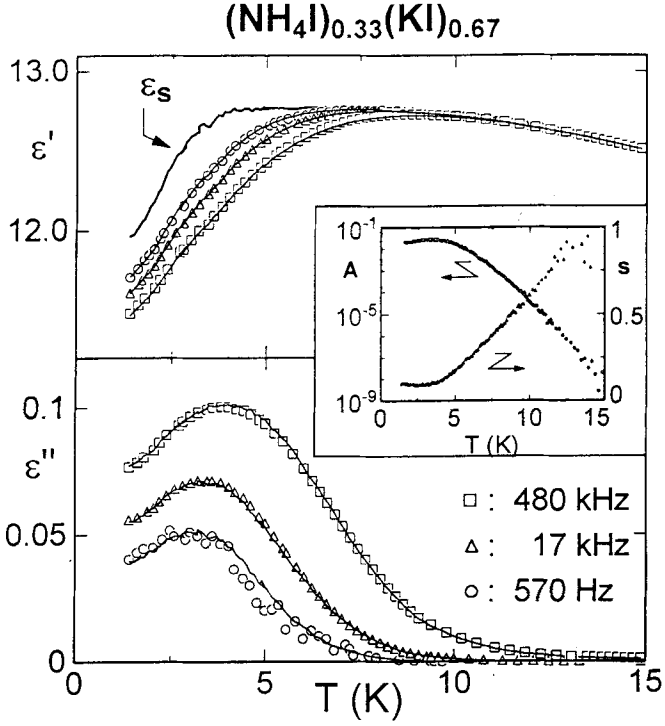

FIGURE 5 Real part (upper frame) and imaginary part (lower frame) of the dielectric constant in $(NH_4I)_{0.33}(KI)_{0.67}$ at three probing frequencies: 480 kHz (□), 17 kHz (△) and 0.57 kHz (○). The solid lines are calculated as described in the test. The thick solid line represents the theoretically extrapolated static susceptibility. The inset shows the fit parameters A and s for this concentration.

extended this analysis to a larger range of frequencies, temperatures and fields. Concerning the imaginary part of the dynamical susceptibility ε'' this mean field theory (MFT) yields the following predictions: i) a sharp increase for small frequencies and fields near the AT line, ii) a frequency dependence $\varepsilon'' \sim \nu^s$, with $s = 0.5$ at the freezing transition and $s \sim 0.25-0.4$ for $T \rightarrow 0$ K and zero fields, and iii) $\varepsilon'' \sim T$ at low temperatures and for all fields.

Of course, MFT does not seem to be adequate to describe the relaxation dynamics below the freezing temperature $T_f(\nu)$. Hence, Fisher and Huse (FH)[23] worked out a phenomenological scaling approach to the static and dynamic properties of finite-range SG. In this picture of the ordered SG phase, the low-lying excitations which dominate the correlations are droplets of coherently flipping spins. According to this scaling approach $\varepsilon'' \sim |\ln \omega\tau_c|^{-(1+\beta)}$. Here $\omega = 2\pi\nu$, τ_c is a microscopic time ($\sim 10^{-12}$ s) and the exponent $\beta \sim 1$, for the most naive assumptions for three-dimensional systems.[23] In the SZ model[21] the dissipative part of the susceptibility should obey a power law, $\varepsilon'' = A\omega^s$, with s of order 0.5. In the droplet model of FH[23] s should be roughly constant over wide ranges of frequency, but with a slight curvature according to $s \sim (1 + \beta)/|\ln \omega\tau_c|$. Assuming $\beta \sim 1$ and $\tau_c \sim 10^{-12}$ s the exponent should change from $s \sim 0.1$ at 1 kHz to $s \sim 0.29$ at 1 GHz. Our experimental results reveal a constant slope for all concentrations and temperatures investigated. Hence we parameterized our data with a pure power-law behavior.

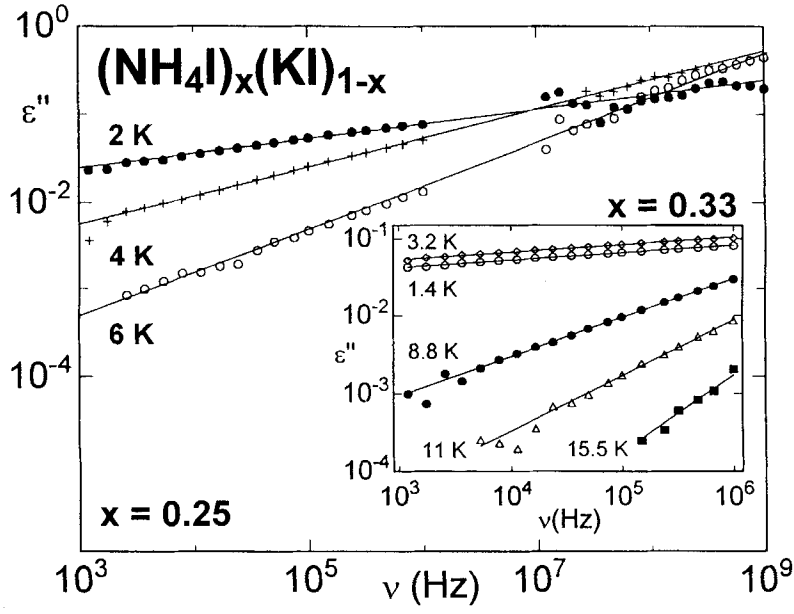

FIGURE 6 $\mathrm{Log}_{10}\varepsilon_2$ vs $\log_{10}\nu$ in $(NH_4I)_{0.25}(KI)_{0.75}$. The solid lines represent power laws, according to $\varepsilon_2 = A\omega^s$. The inset shows similar results for $(NH_4I)_{0.33}(KI)_{0.67}$ obtained in the audiofrequency range.

Accordingly the complex dielectric constant can be described using $\varepsilon^* = \varepsilon_s - 2A(T)\omega^{s(T)}/\pi/s(T) + iA(T)\omega^{s(T)}$. Here ε_s is the static dielectric constant and the real and imaginary parts are strictly related via the Kramers-Kronig transformation. The solid lines drawn in Figures 5 and 6 through the data points represent the results of fits of this model to the experimental data, using the parameters $A(T)$, $s(T)$ and ε_s. ε_s is indicated as thick solid line in the upper frame of Figure 5. The temperature dependences of the parameters A and s, for all $(NH_4I)_x(KI)_{1-x}$ crystals investigated in the glassy regime g_2, are presented in Figure 7 (see also inset of Figure 5). $A(T)$ reveals a cusp-like maximum. The maximum value of A, for a given concentration, closely corresponds to the maximum in $\varepsilon''(T)$ which defines the freezing temperature T_g. On the high-temperature side, A steadily decreases over many orders of magnitude (for $x = 0.33$ see inset in Figure 5). The frequency exponent s decreases with decreasing temperatures and yields a limiting low-temperature value $s \sim 0.07$. For all x, this limiting value of s is reached at the cusp maximum of $A(T)$. This means, that below the freezing transition the apparent frequency exponents are in reasonable agreement with the predictions of the FH droplet model in the audiofrequency range, but are much smaller than those of order 0.5 predicted by the SZ model. However, in contradiction to the FH model we find no experimental evidence for frequency dependent exponents s. The value of $s = 0.5$, as predicted in the SZ model at T_f is reached far above T_f. The SZ predictions for s $(T < T_f) = 0.5 - (T_f - T)/T_f/\pi$ are indicated in Figure 4 by solid lines, the predictions for s $(T = 0)$ by arrows.

Finally, we would like to comment on the freezing dynamics. As can be seen in Figure 2, the peak maximum in $\epsilon''(T)$ slightly shifts towards lower temperatures with decreasing frequencies. Defining the frequency of the peak maximum as mean relaxation rate, the slowing down of these rates follows on Arrhenius law $\nu = \nu_0$

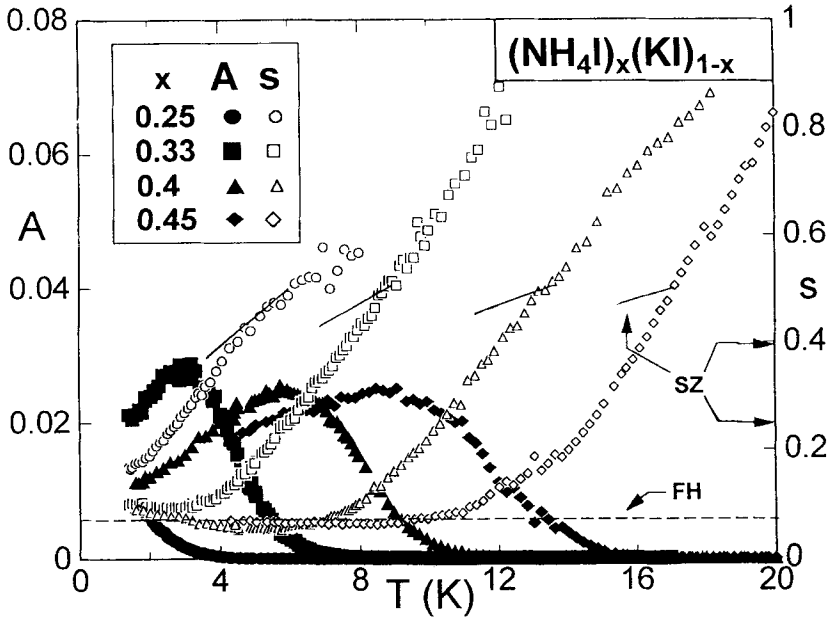

FIGURE 7 Temperature dependence of the parameters A (solid symbols) and s (open symbols), as determined in $(NH_4I)_x(KI)_{1-x}$ for concentrations $x = 0.25$, 0.33, 0.4 and 0.45. The solid lines indicate the predictions of the SZ model at $T \leq T_f$. The arrows indicate the limiting zero temperature results. The dashed line is the FH result as explained in the text.

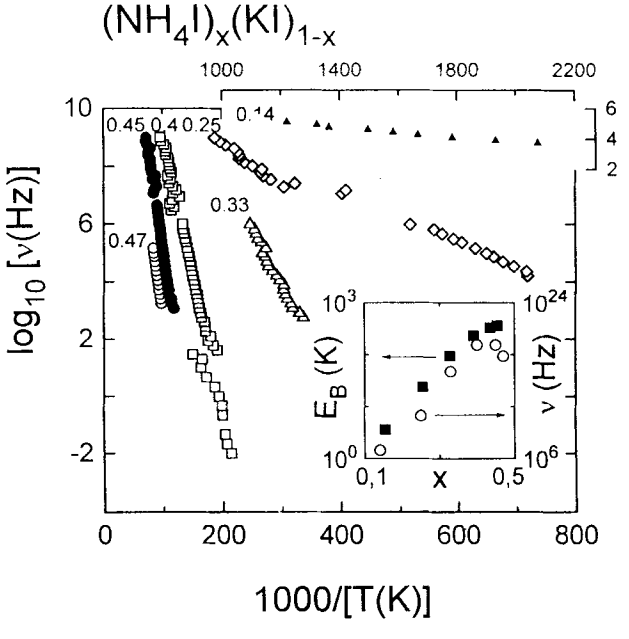

FIGURE 8 Temperature dependence of the frequency of the loss maximum (characteristic relaxation rate) for all concentrations shown in an Arrhenius-type representation.

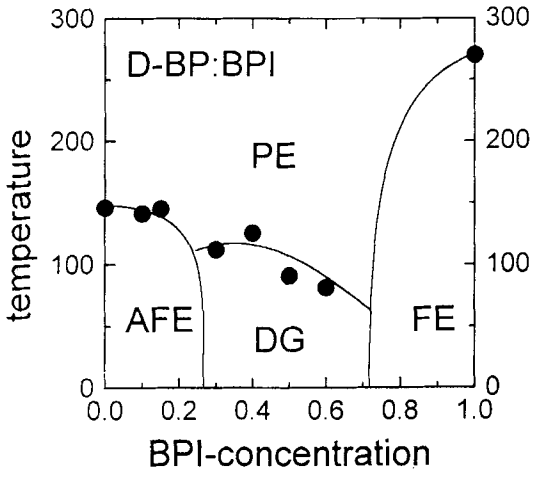

FIGURE 9 (x, T)-phase diagram of D-BP:BPI. The lines are drawn to guide the eye.

$\exp(-E_B/k_BT)$ for all concentrations (Figure 8). The energy barriers are of order 10 K for $x < 0.25$ but increase strongly towards higher concentrations, reaching $E_B \sim$ 350 K at $x = 0.45$ (inset of Figure 8). The attempt frequencies ν_0 reveal physically plausible microscopic rates only for $x < 0.25$. Note that they reach values of order 10^{20} s^{-1} for the higher concentrations (inset of Figure 8), showing that a parametrization in terms of an activated behavior is not meaningful. This again demonstrates unambiguously, that the relaxation dynamics for $x < 0.25$ is due to thermally activated reorientations of isolated ammonium molecules, while the relaxational behavior in the glass regime g_2 is characteristic for the near-equilibrium dynamics of a glass phase.

2.2 *Betaine Proton Glasses*

As stated in the introduction, the proton glasses which have been investigated most thoroughly belong to the KDP family.[7] Compounds with the general formula $(AH_2XO_4)_{1-x}(NH_4H_2XO_4)_x$ (A = K, Rb, Cs and X = P, As) and their deuterated isomorphs have been investigated. In these crystals the acid protons form a three-dimensional network of hydrogen bonds. At high temperatures the protons are dynamically disordered in their double-well potentials. In certain ranges of composition x the proton motion freezes out on lowering the temperature, undergoing a transition into a dipolar glass state.

Dipolar glass states have also been reported to occur in mixtures of betaine phosphate (BP) and betaine arsenate,[25] as well as in solid solutions of BP and betaine phosphite (BPI).[26–28] Also deuterated compounds have been investigated.[29,30] In these crystals the inorganic groups, PO_4 and PO_3 respectively, are linked by hydrogen bonds in a chainlike fashion. Therefore these systems are candidates for the application of one-dimensional polar models.[31] In this article we focus on a solid solution of deuterated betaine phosphate $[(CH_3)_3\ NCH_2\ COOD_3\ PO_4]$ (D-BP) and deuterated betaine phosphite $[(CH_3)_3NCH_2COOD_3PO_3]$ (D-BPI). We will discuss in detail the linear and non-linear susceptibilities in the mixed crystal $(D\text{-}BP)_{0.4}$ $(D\text{-}BPI)_{0.6}$, abbreviated as

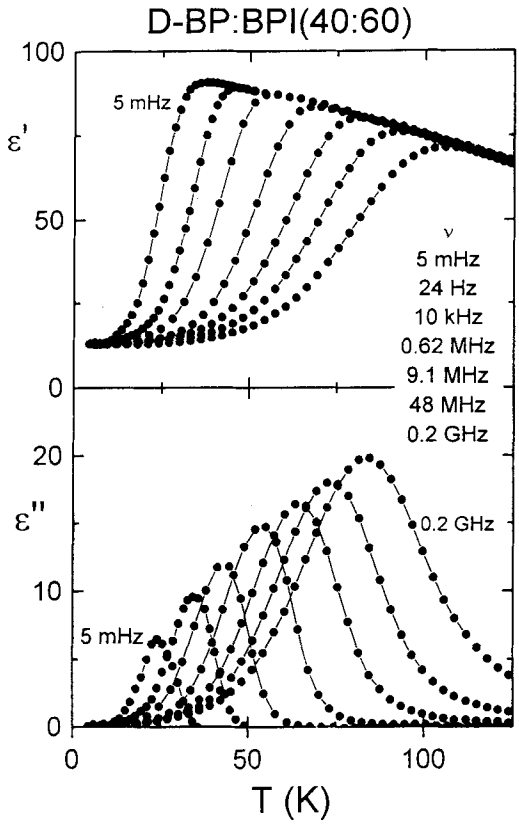

FIGURE 10 Temperature dependence of the real, ε' (upper frame), and imaginary part, ε'' (lower frame), of the dielectric constant in D-BP:BPI (40:60) at frequencies from $5 \cdot 10^{-3}$ Hz to 0.2 10^9 Hz. The lines are drawn to guide the eye.

D-BP:BPI (40:60). Figure 9 shows a preliminary phase diagram of D-BP:BPI. Between the low-temperature ordered phases of AFE BP and FE BPI a broad glassy regime shows up.

Figure 10 shows the temperature dependence of real and imaginary part of the dielectric constant, $\varepsilon^* = \varepsilon' - i\varepsilon''$, taken at different frequencies between 5 mHz and 0.2 GHz. The steplike decrease of ε' and the loss peak in ε'' reveal the slowing down of the dipolar degrees of freedom on the time scale of the experiment. The dipolar degrees of freedom are directly connected with the jumps of the acid protons within the double-well potentials of the hydrogen bonds. Figure 11 shows the same set of data transformed onto a frequency scale. Here we plotted the complete frequency range from 10^{-3} Hz $\leq \nu \leq 10^9$ Hz. From the shape and the temperature shift of the loss peaks it becomes clear that the mean relaxation rate slows down dramatically and that, at the same time, the distribution width increases dramatically. However, Figure 11 provides experimental evidence that the distribution of relaxation rates broadens almost symmetrically. Hence we fitted the data with a Cole-Cole expression, which introduces, in addition to the parameters of the pure Debye relaxation, a single width parameter α. Fits using the Cole-Cole type function are shown as solid lines in Figure 11. Within the experimental uncertainties the experimental re-

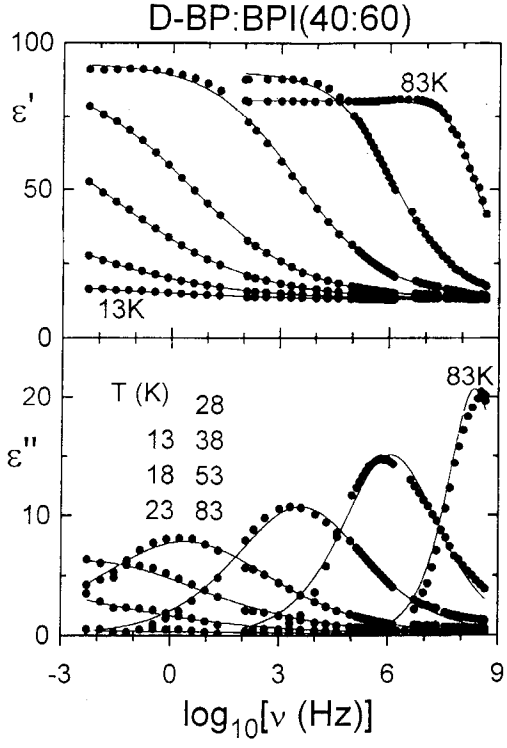

FIGURE 11 Frequency dependence of ε′ (upper frame) and ε″ (lower frame) in D-BP:BPI (40:60) at different temperatures between 13 K and 83 K. The solid lines are calculated using Cole-Cole-fits.

sults are well described. However, at high temperatures asymmetric contributions are clearly visible and a careful lineshape analysis in protonated compounds has been performed recently.[32] The width parameter α increases steadily with decreasing temperature ($\alpha = 0.11$ at $T = 93$ K and reaches $\alpha = 0.53$ at $T = 53$ K). This type of behavior can well be reproduced using a temperature independent Gaussian distribution of energy barriers which yields a width that increases proportional to T^{-1}. We have demonstrated recently[32] that in the betaine proton glasses the shape of the loss peaks is determined predominantly by a Gaussian distribution of energy barriers. The asymmetry in the distribution of relaxation times plays only a minor role.[32]

The mean relaxation rate follows approximately an activated type of behavior (solid triangles in Figure 12) with an energy barrier $E_B = 807$ K and attempt frequency $\nu_0 = 5 \cdot 10^{12}$ Hz. Clearly, the relaxation processes in BP:BPI are polydispersive and obviously, the mean relaxation rates do not diverge at finite temperatures. Despite that fact, the question remains whether it is possible and meaningful to determine an equilibrium phase transition temperature into a glass phase. The rest of this section deals with concepts and experimental realizations to answer this question.

In KDP-type proton glasses experimental evidence has been provided that the mean relaxation rate follows a Vogel-Fulcher law $\nu = \nu_0 \cdot \exp[E_B/k_B.(T - T_{VF})]$ with an attempt frequency ν_0, a hindering barrier E_B and a Vogel-Fulcher temperature T_{VF}.[33] At the same time, an extrapolation of the width of the loss peaks indicated a

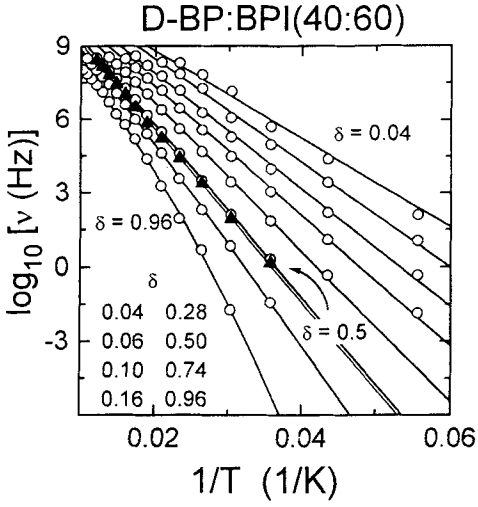

FIGURE 12 Arrhenius representation of the reduced dielectric constant δ in D-BP:BPI (40:60) ($0.04 \leq \delta \leq 0.96$) according to the procedure suggested by Kutnjak *et al.*[34] Experimental results: empty circles; mean relaxation rate as determined from the Cole-Cole fits of Figure 9 (solid triangles). The solid lines were calculated using Arrhenius laws for $\delta > 0.5$ and using Vogel-Fulcher laws for $\delta \geq 0.74$: $\delta = 0.74$: $T_{VF} = 3$ K; $\delta = 0.96$: $T_{VF} = 10$ K.

divergence close to T_{VF}.[33] The concept that the maximum relaxation time diverges at a finite temperature has been tested in full detail by Kutnjak *et al.*[34] They proposed a novel frequency-temperature plot of the real part of the dielectric constant to demonstrate that the low-frequency edge of the distribution of relaxation times diverges at a finite temperature. They plotted $\delta = (\varepsilon' - \varepsilon_\infty)/(\varepsilon_s - \varepsilon_\infty)$ in an Arrhenius type of representation and showed that the resulting plots follow an Arrhenius behavior for $\delta \ll 1$ and a Vogel-Fulcher behavior for $\delta \approx 1$. As δ varies from 0 to 1, ε′ shifts from ε_∞ to ε_s and hence, for $\delta = 1$ the low frequency edge of the distribution of relaxation times is followed. This type of representation for D-BP:BPI (40:60) is shown in Figure 12, for δ values $0.04 \leq \delta \leq 0.96$. While a pure Arrhenius behavior describes the data satisfactorily well for $\delta \leq 0.74$ a clear Vogel-Fulcher type of behavior is observed for $\delta = 0.96$. An extrapolation of these data to $\delta = 1$ yields a finite critical temperature, where the maximum relaxation time diverges close to $T_0 \sim 30$ K. It is interesting to note that the curve characteristic for $\delta = 0.5$, follows the temperature dependence of the characteristic relaxation rate (solid triangles).

It is generally believed that the Almeida-Thouless (AT) line for spin glasses in an external magnetic field, which separates the ergodic high-temperature phase from the non-ergodic glass phase, can be determined through measurements of the field cooled (FC) and the zero-field cooled (ZFC) susceptibilities. The two quantities are expected to split at the AT line and should be significantly different in the glass phase. Figure 13 shows the results of the experimentally determined polarization during a ZFC, field-heated (FH), FC and zero-field heated (ZFH) measuring cycle. FC and FH polarizations are equal for $T > 30$ K, but for $T < 30$ K the FC values are significantly above the ZFH values. From these experiments a quasi-static glass transition temperature of 30 K would follow. Similar experiments have been performed on a deuterated RADP glass by Levstik *et al.*[35]

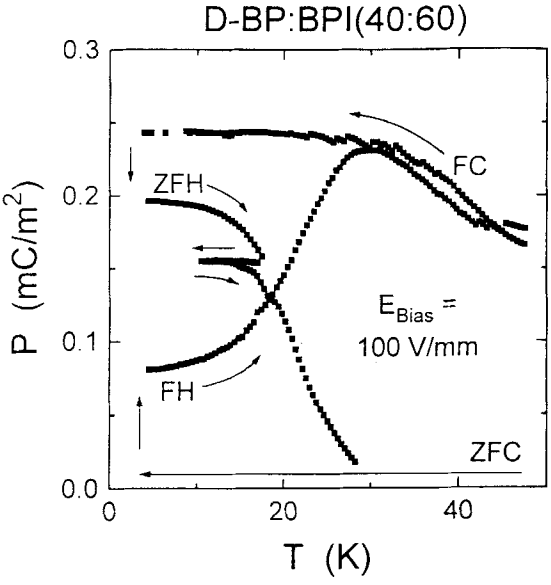

FIGURE 13 Polarization in D-BP:BPI (40:60) as determined in field cooled (FC) and zero-field cooled experiments. The arrows represent the order in which the experiments were performed.

It has been recognized long time ago that the linear susceptibility is not the best suited quantity in order to study the nature of the glass transition. One should rather investigate the spin glass susceptibility χ_{SG} which plays the same role in a spin glass as the uniform susceptibility in a ferroelectric material.[3,34] For small external fields, χ_{SG} is related to the nonlinear susceptibility χ_{nl} which exhibits a critical singularity at the glass transition temperature. For finite fields the nonlinear susceptibility includes also higher order terms and in general differs from χ_{SG}. In D-BP:BPI (40:60) we tried to determine the nonlinear susceptibility using two different experimental routes. We measured hysteresis loops, $P(E)$ using a maximum voltage of 1 kV/mm and analyzed the data in terms of an expansion of the polarization P in powers of the external field, i.e.

$$P = \chi_1 E + \chi_2 E^2 + \chi_3 E^3 + \cdots.$$

In the absence of symmetry breaking local fields, on the basis of naive field reversal arguments $\chi_2 = 0$ is expected. However, it has been shown by Vollmayr *et al.*[37] that in a three-state Potts-glass χ_2 does not vanish. Figure 14 shows the result of this type of analysis. Here the real part of expansion coefficients χ_1, χ_2 and χ_3 and the corresponding loss angles, δ_1, δ_2 and δ_3 are shown. χ_1 closely resembles the linear susceptibility, determined at low frequencies (see Figure 1, upper frame). We obtain a finite χ_2, which however, could also indicate local electric fields and finally we observed a cusp-like χ_3, with a cusp maximum at approximately 28 K.

In a second experiment we determined the nonlinear susceptibility using an ac-technique with $\nu = 90$ Hz in a bias field of 1000 V/mm. We determined χ_3 from a comparison with the linear susceptibility χ_1, neglecting contributions due to χ_2. The result is shown in Figure 15. Again χ_{nl} reveals a sharp cusp-like singularity close to 30 K. It is important to note that in the temperature regime in which the nonlinear

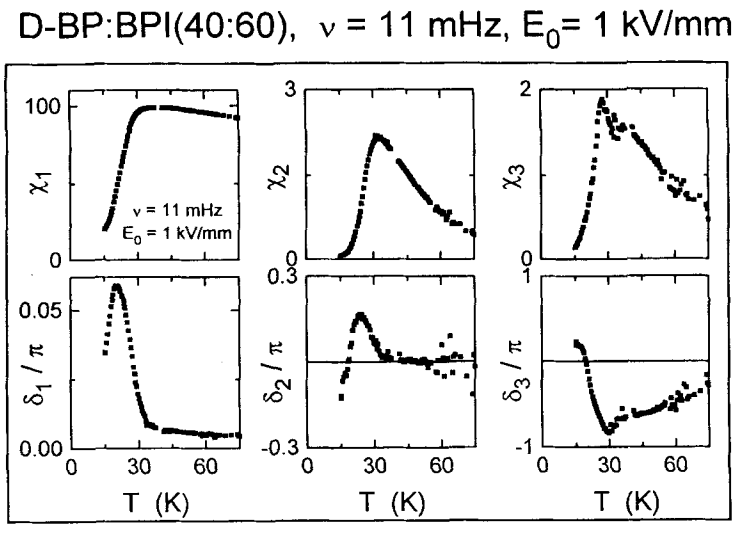

FIGURE 14 Absolute values of the susceptibilities χ_1, χ_2 and χ_3 and loss angles δ_1, δ_2 and δ_3 versus temperature, observed in D-BP:BPI (40:60).

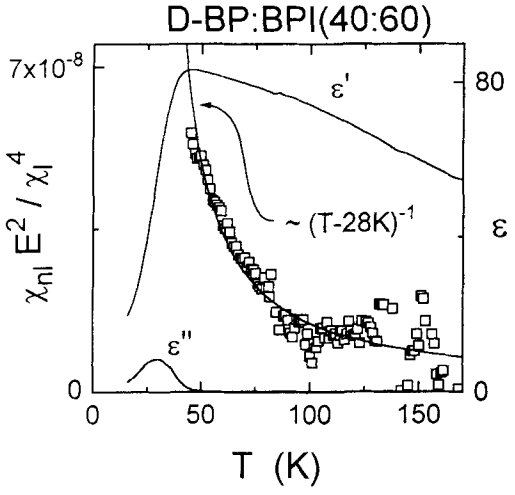

FIGURE 15 Temperature dependence of the nonlinear susceptibility χ_{nl} in D-BP:BPI (40:60). The solid line represents a fit to power laws as indicated.

susceptibility strongly increases the linear susceptibility is almost flat. We analyzed the temperature dependence using a scaling ansatz $\chi_3 \sim \chi_1^4 (T - T_g)^{-\gamma}$. The solid line in Figure 15 shows the result of a fit, using a fixed value of the exponent γ = 1. From this fit a value of T_g = 28 K has been determined.

3. CONCLUSIONS

In this review we have presented detailed dielectric results from two dipolar glass systems. The (x, T)-phase diagram of $(NH_4I)_x(KI)_{1-x}$ is characterized by a striking

polymorphism and, even more amazing, by a polyamorphism in its glassy regime. The dielectric loss in the glass phase g_2 is characterized by a pure power-law behavior $\varepsilon'' \sim \nu^s$. We tried to compare our data with existing theoretical models. The relaxation dynamics in g_1 is most probably dominated by single ion reorientations, while up to now nothing can be said concerning the glass phase g_3.

The dynamics of the hydrogen bonds in the proton glass D-BP:BPI (40:60) reveals a purely relaxational behavior. Here we investigated the nonlinear susceptibilities and compared FC and ZFC results. From these experiments a glass transition temperature $T_g = 28\ \text{K} \pm 2\ \text{K}$ can be determined which is in rough agreement with the temperature at which the low-frequency edge of the relaxation spectrum diverges.

ACKNOWLEDGEMENTS

This work was supported by the Deutsche Forschungsgemeinschaft via the SFB 262/project D5. We thank A. Maiazza for growing the high-quality single crystals used in this work.

REFERENCES

1. K. Binder and A. P. Young, *Rev. Mod. Phys.*, **58,** 801 (1986).
2. U. T. Höchli, K. Knorr and A. Loidl, *Adv. Phys.*, **39,** 405 (1990).
3. K. Binder and J. D. Reger, *Adv. Phys.*, **41,** 547 (1992).
4. W. Känzig, H. R. Hart, Jr. and S. Roberts, *Phys. Rev. Lett.*, **13,** 543 (1964).
5. M. Paasch, M. Winterlich, R. Böhmer, R. Sonntag, G. J. McIntyre and A. Loidl, *Z. Physik*, (1996) in print.
6. For example, see: D. Rytz, U. T. Höchli and H. Bilz, *Phys. Rev. B*, **22,** 359 (1980).
7. E. Courtens, *Helv. Phys. Acta.*, **56,** 705 (1983); H. Terauchi, *Phase Trans.*, **7,** 315 (1986).
8. N. G. Parsonage and L. A. K. Stavely, in "Disorder in Crystals," Clarendon Press, Oxford 1978, pp. 311–388.
9. C. H. Perry and R. P. Lowndes, *J. Chem. Phys.*, **51,** 3648 (1969).
10. R. Havighurst, E. Mack, Jr. and F. C. Blake, *J. Am. Chem. Soc.*, **47,** 29 (1925).
11. C. C. Stephenson, L. A. Landers and A. G. Cole, *J. Chem. Phys.*, **20,** 1044 (1952).
12. C. Bostoen, G. Coddens and W. Wegener, *J. Chem. Phys.*, **91,** 6337 (1989).
13. I. Fehst, R. Böhmer, W. Ott, A. Loidl, S. Haussühl and C. Bostoen, *Phys. Rev. Lett.*, **64,** 3139 (1990).
14. M. Paasch, G. J. McIntyre, M. Reehuis, R. Sonntag and A. Loidl, *Z. Physik B* (1995) in print.
15. J.-F. Berret, C. Bostoen, J.-L. Sauvajol, B. Hennion and S. Haussühl, *Europhys. Lett.*, **16,** 91 (1991); -F. Berret, J.-L. Sauvajol and B. Hennion, *J. Phys. Condens, Matter*, **4,** 9235 (1992); J.-F. Berret, S. Ravy and B. Hennion, *J. Phys. I (France)*, **3,** 1031 (1993).
16. T. Umeki, K. Yagi and H. Terauchi, *J. Phys. Soc. Jap.*, **63,** 876 (1994).
17. R. Böhmer, F. Fujara and G. Hinze, *Sol. State Commun.*, **86,** 183 (1993).
18. R. Blinc, T. Apih, J. Dolinsek, M. Sprogar and B. Zalar, preprint (1995).
19. G. H. Wolf, S. Wang, C. A. Herbst, D. J. Durben, W. F. Oliver, Z. C. Kang and C. Halvorsen, in "High Pressure Research: Application to Earth and Planetary Sciences," Y. S. Manghuani and M. H. Manghuani, eds., Terra Scientific Publ., Tokyo/Washington, 1992, pp. 503–517.
20. C. A. Angell, P. H. Poole and J. Shao, preprint.
21. C. C. Paulsen, S. J. Williamson and H. Maletta, *Phys. Rev. Lett.*, **59,** 128 (1987).
22. H. Sompolinsky and A. Zippelius, *Phys. Rev. B*, **25,** 6860 (1982).
23. D. S. Fisher and D. A. Huse, *Phys. Rev. B*, **38,** 373 (1988) and *Phys. Rev. B*, **38,** 386 (1988).
24. K. A. Fischer and W. Kinzel, *J. Phys. C*, **17,** 4479 (1984).
25. M. Maeda, *Ferroelectrics*, **96,** 269 (1989).
26. M. L. Santos, J. C. Azevedo, A. Almeida, M. R. Chaves, M. R. Pires, H. E. Müser and J. Albers, *Ferroelectrics*, **108,** 363 (1990); M. L. Santos, M. R. Chaves and A. Almeida, *Ferroelectrics Lett.*, **15,** 17 (1993).
27. S. L. Hutton, I. Fehst, R. Böhmer, M. Braune, B. Mertz, P. Lunkenheimer and A. Loidl, *Phys. Rev. Lett.*, **66,** 1990 (1991); S. L. Hutton, I. Fehst, R. Böhmer and A. Loidl, *Ferroelectrics*, **127,** 279 (1992).
28. J. Banys, C. Klimm, G. Völkel, H. Bauch and A. Klöpperpieper, *Phys. Rev. B*, **80,** 16 751 (1994).

29. J. Hemberger, P. Lunkenheimer, H. Ries and A. Loidl, preprint.
30. J. Albers, A. Klöpperpieper, H. E. Müser and H. J. Rother, *Ferroelectrics*, **54**, 45 (1984).
31. M. Oresic and R. Pirc, *Phys. Rev. B*, **47**, 2655 (1993).
32. H. Ries, R. Böhmer, I. Fehst and A. Loidl, *Z. Physik B*, 1995 in print.
33. E. Courtens, *Phys. Rev. Lett.*, **52**, 69 (1984); H. J. Brückner, E. Courtens and H. G. Unruh, *Z. Physik B*, **73**, 337 (1988).
34. Z. Kutnjak, C. Filipic, A. Levstik and R. Pirc, *Phys. Rev. Lett.*, **70**, 4015 (1993).
35. A. Levstik, C. Filipic, Z. Kutnjak, I. Leostik, R. Pirc, B. Tadic and R. Blinc, *Phys. Rev. Lett.*, **66**, 2368 (1991).
36. R. Pirc, B. Tadic and R. Blinc, *Physica B*, **193**, 109 (1994).
37. K. Vollmayr, G. Schneider, J. D. Reger and K. Binder, *J. Non-Cryst. Solids*, **172–174**, 488 (1994).